JACS
JOURNAL OF THE AMERICAN CHEMICAL SOCIETY
Article
Cite This: J. Am. Chem. Soc. XXXX, XXX, XXX−XXX
pubs.acs.org/JACS

Disodium Salts of Pseudoephedrine-Derived Myers Enolates: Stereoselectivity and Mechanism of Alkylation

Yuhui Zhou, Ivan Keresztes, Samantha N. MacMillan, and David B. Collum*

Department of Chemistry and Chemical Biology, Baker Laboratory, Cornell University, Ithaca, New York 14853−1301, United States

Supporting Information

ABSTRACT: Pseudoephedrine-derived dianionic Myers enolates were generated using sodium diisopropylamide (NaDA) in THF solution. The reactivities and selectivities of the disodium salts largely mirror those of the dilithium salts but without the requisite large excesses of inorganic salts (LiCl) or mandated dilute solutions. The disodium salts require careful control of temperature to preclude deleterious aggregate aging effects traced to changes in the aggregate structure and intervening O-alkylations. Structural studies and density functional theory (DFT) computations show a dominant highly symmetric polyhedron quite different from the lithium analogue. No enolate−NaDA mixed aggregates are observed with excess NaDA. Rate studies show an alkylation mechanism involving an intervening tetramer−monomer pre-equilibrium followed by rate-limiting alkylation of tetrasolvated monomers. DFT computations were conducted to explore the possible influences on stereochemistry. A crystal deriving from samples aged at ambient temperature contains six dianionic subunits and two monoanionic (alkoxide-only) subunits. A new preparation of concentrated solutions of NaDA in THF solution is described.

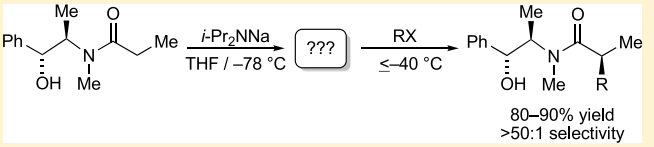

INTRODUCTION

Myers and co-workers have shown that dianions of type **2**, derived from acylated pseudoephedrines (**1**) and lithium diisopropylamide (LDA), alkylate with high yields and stereoselectivities (eq 1).[1] Alkyl halides and epoxides add

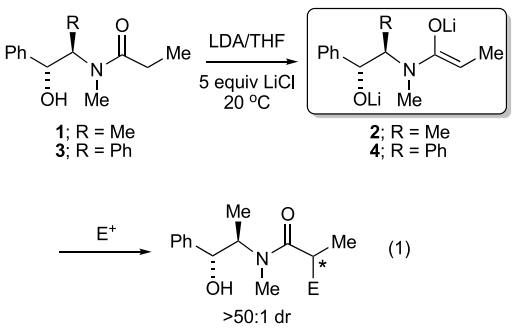

with opposite facial selectivities for reasons that are not yet understood. Removal of the pseudoephedrine auxiliary is facilitated by anchimeric assistance.[2] Second-generation enolates (**4**) based on a diphenyl-substituted amino-ethanol backbone (**3**) are also effective, obviating the need to work with a controlled substance.[3] Of note, however, both protocols require the addition of ≥5.0 equiv of anhydrous LiCl, which imposes relatively low (∼0.10 M) enolate concentrations. These two limitations, while of minor inconvenience in an academic setting, add significant cost on pharmaceutical plant scales.[4]

We previously examined the structures and reactivities of **2**. The low conversions in the absence of LiCl were traced to aging effects, in which an exceedingly complex mixture of ill-defined, but highly reactive, aggregates converge to a single inert octalithiated aggregate.[5] Of several possible 16-vertex polyhedra (Chart 1),[6] **2** was shown to have a core corresponding to **5** (M = Li). Enolate **2** in the presence of 5.0 equiv of LiCl forms a mixed aggregate that eluded our best efforts at assignment but displayed high reactivities and excellent overall yields, as previously described by Myers.

Chart 1. Polyhedra of Octametalated Species[a]

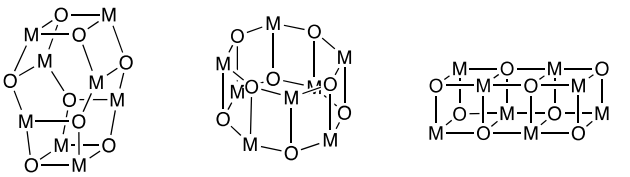

[a]M = Li or Na.

We sought to develop a modified alkylation protocol that would omit the LiCl from the reaction mixture. Although the unaged, LiCl-free enolates were orders of magnitude more reactive than the corresponding aged samples containing exclusively **5**, we were unable to coax alkylations beyond 70% conversion, owing to the onset of aging.[7,8] Thus, a LiCl-free alkylation protocol seemed to call for a fundamentally different strategy.

Received: July 30, 2019

DOI: 10.1021/jacs.9b08176
J. Am. Chem. Soc. XXXX, XXX, XXX−XXX

We describe herein the chemistry of disodiated enolate **8**, generated using sodium diisopropylamide (NaDA) in THF. Alkylations proceed in high yields and selectivities at up to 0.50 M enolate without added salts (eq 2). We document two

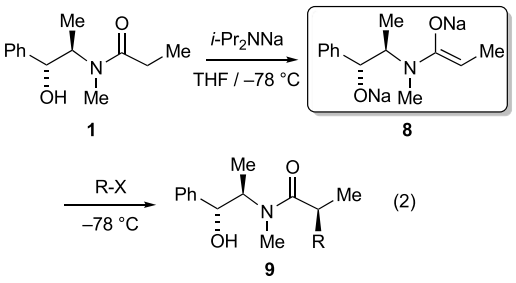

distinct aging effects that influence structure and reactivity, but both are mitigated through adequate temperature control. Structural studies reveal that unaged disodium enolate **8** is tetrameric, with either an octagonal prismatic or a stacked-cube core (Chart 1, **6** or **7**). Rate and computational studies reveal the mechanism of alkylation.[9,10] A new preparation of 1.6–1.8 M NaDA directly in THF solution is also notable.

RESULTS AND DISCUSSION

NaDA Preparation. The NaDA used in these studies was prepared according to several different methods. We had previously modified[11a] a procedure first reported by Wakefield[12] involving reduction of diisopropylamine with sodium dispersion and isoprene. Although Wakefield originally deposited solid NaDA, we generate 1.0 M solutions of NaDA in *N*,*N*-dimethylethylamine (DMEA) that can be stored for months with refrigeration. For the structural and rate studies, we recrystallize and store solid NaDA with refrigeration, but this added precaution does not significantly affect reactivity.[11] A benchtop protocol using NaDA/DMEA with added THF, however, was not effective owing to an unusually high (third-order) THF dependence (vide infra).

We explored benchtop procedures that would require no specialized inert atmosphere equipment. Under Lochmann's conditions in which *n*-BuNa is precipitated by adding *n*-BuLi to *tert*-BuONa in hexanes before adding diisopropylamine, we encountered problems in decanting the supernatant owing to the finely divided precipitate.[13] The Wakefield protocol involving sodium dispersion mediated by isoprene was readily adapted to neat THF to afford up to 1.7 M stock solutions of NaDA that are stable for same-day use, provided that they are kept at 0 °C ($t_{1/2}$ = 1.0 h at 25 °C in neat THF; $t_{1/2} \gg 5$ h at 0 °C in neat THF).[11b,14] However, the sodium dispersion made the decanting step challenging.

The optimized preparation entailed using freshly cut large pieces of sodium (>100 mg) that are often more available than the dispersion, and the decanting is trivial requiring no special precautions. The reaction is stirred at 0 °C for 45 min. Empirically, when the reaction is finished, the shiny sodium surface darkens. There is one critical and somewhat unexplainable protocol: the supernatant must be removed from the sodium when the reaction is complete to prevent formation of a gel accompanied by graying (possibly NaH), which becomes visible within several hours. Once the supernatant is added to a new vessel, it can be stored at 0 °C for at least 5 h or at −20 °C for 24 h without gelling or measurable loss of titer. The titer drops by 5% within 48 h at −20 °C. If stored at −20 °C, warming to 0 °C makes the solution less viscous and easily syringed. Given that the THF solution of NaDA can be placed over fresh sodium without evidence of gelling, we infer that the surface of the spent sodium must somehow be important, and possibly the isoprene dimer byproduct is involved. Titration with diphenylacetic acid[15] routinely showed 1.6–1.8 M titer (approximately 80–90% of the theoretical titer). The entire preparation requires approximately an hour. We have prepared 200 mmol with no evidence of an exotherm, but suggest monitoring the internal reaction temperature in case an exotherm emerges.

Reactivity and Selectivity. Exposure of **1** (0.040 M) to 2.5 equiv of NaDA in neat THF at −78 °C leads to the disappearance of the IR absorbance of **1** at 1649 cm^{-1} and its replacement with the absorbance of disodium enolate **8** at 1620 cm^{-1} within 3 min. At higher temperatures, deleterious enolate aging effects intervene (vide infra). Quantitative monitoring of the alkylation of **8** by IR spectroscopy is challenging owing to overlapping absorbances; however, ^{1}H NMR spectroscopy reveals that alkylations with 2.0 equiv of highly reactive alkyl halides, such as benzyl bromide (Table 1, entry 1) or allyl bromide (entry 2), occur within 5 min at −78 °C. Less reactive saturated alkyl halides such as *n*-BuI (entry 4) require elevated temperatures (−40 °C) or protracted reaction times. *n*-BuBr requires 48 h at −78 °C to attain high conversion (entry 3). Even the shortened reaction times for the alkyl iodides showed some sacrifice of percent conversion and consequent erosion of isolated yield. Attempts to force such recalcitrant alkylations with excessive warming cause O-alkylations (**10** and **11**), which can be largely mitigated by controlling temperature and minimizing the excess of alkylating agent. Product assignments in Table 1 were based on those reported by Myers.[1] We hasten to add that the isolated yields reported in Table 1 are *not* corrected for recovered starting material.

Table 1. Alkylation of Enolate 8 (Equation 2)

entry	R–X	temp, time	selectivity	% conv	yield
1	BnBr	−78 °C, 10 min	>50:1	>99%	96%
2	allyl bromide	−78 °C, 10 min	>50:1	94%	90%
3	*n*-BuBr	−78 °C, 48 h	>50:1	94%	92%
4	*n*-BuI	−40 °C, 1.0 h	>50:1	92%	88%
5	*i*-BuI	−40 °C, 2.0 h	>50:1	84%	80%
6	$BrCH_2CO_2$-*t*-Bu	−78 °C,[a] 3.5 h	>50:1		<50%

[a]With slow warming to 20 °C.

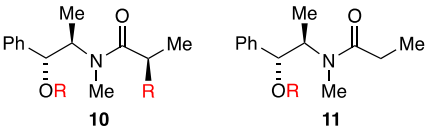

We observed a reversal of stereochemistry in the epoxide addition, as previously reported by Myers in the context of the lithium enolates (eq 3). Once again, the modest yields trace to

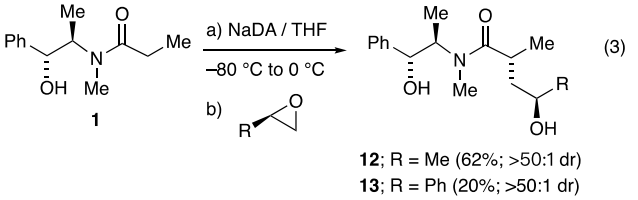

DOI: 10.1021/jacs.9b08176
J. Am. Chem. Soc. XXXX, XXX, XXX–XXX

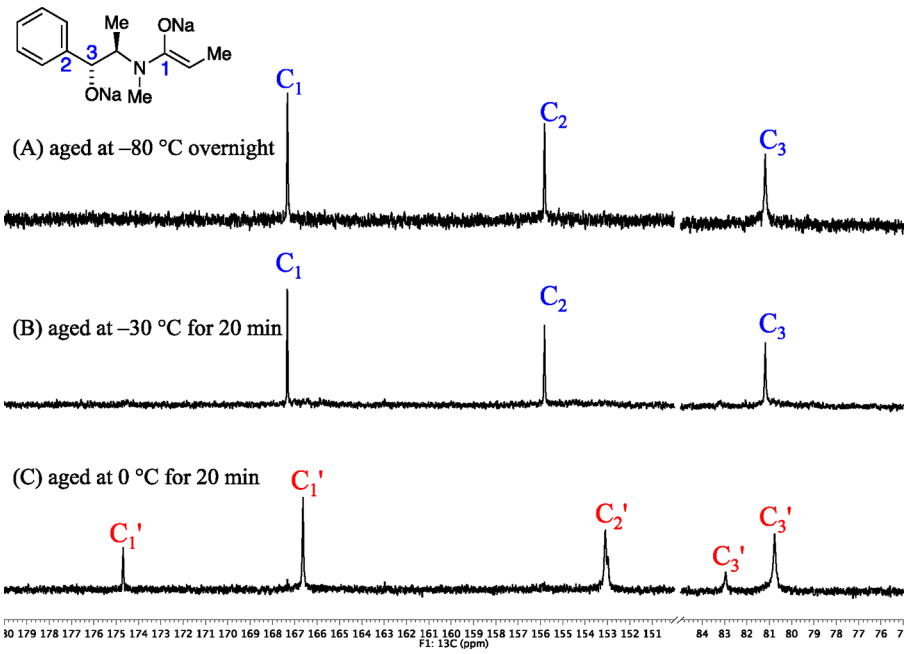

Figure 1. Partial $^{13}C\{^{1}H\}$ NMR spectra of a solution of 0.30 M **8** in neat (12.3 M) THF-d_8 recorded at −80 °C: (A) aged at −80 °C overnight; (B) aged at −30 °C for 20 min; and (C) aged at 0 °C for 20 min.

incomplete conversion, but in these reactions, the losses are considerable. Fortunately, excess epoxide does not cause O-alkylation; thus we could allow the samples to warm to force higher percent conversions. The highest yields were obtained when the reaction was warmed from −80 to 0 °C over a period of 18 h. However, the Myers lithium-based protocol provides decidedly higher yields.

The incomplete conversions are part of a complex story described below, but preliminary comment is warranted here. Before we appreciated the importance of temperature control, we often recovered significant (20−30%) starting material, which was baffling. We initially suspected competitive dehydrohalogenations of the alkyl halides by the disodiated enolate, but alkenes were not observed by NMR spectroscopy or GC, provided that we took precautions to avoid residual NaDA. In fact, the nearly instantaneous dehydrohalogenation[11c] acts to quench excess NaDA, with the resulting alkene being diagnostic of adequate titers. Efforts to force alkylations in aged samples by raising the temperature afforded low levels (<10%) of byproducts such as **10** and **11**, deriving from O-alkylation. O-Alkylation is particularly acute when NaDA is replaced with NaHMDS, suggesting that reversible proton transfer may somehow be involved. *tert*-Butyl bromoacetate (entry 6) seemed particularly problematic; with this substrate, control of both stoichiometry and temperature provided only modest conversion and O-alkylated side products, with isolated yields of the desired product in an erratic 20−50% range. The potential acidity of *tert*-butyl bromoacetate reinforces suspicions that reversible proton transfer is at play.[16]

Solution Structure. The acute challenges of characterizing dianions[17] are exacerbated by the absence of M−O scalar coupling to study aggregation and M−N scalar coupling to probe Na−N contacts. ($^{6}Li-^{15}N$ couplings were detected in lithium enolate **2**, for example.[5]) We used the method of continuous variations (MCV)[18] to determine the degree of aggregation of disodium salt **8** and standard 2D-NMR spectroscopies (COSY, HMBC, HSQC, NOESY, and ROESY)[19] to establish critical spatial relationships. Density functional theory (DFT) computations at the M06-2X level of theory were conducted for both geometry optimizations and single-point calculations. The standard 6-31G(d) basis set was used for geometry optimizations whereas the expanded basis set 6-311+G(2d,p) was used for single point calculations.[20,21] Most of these data are archived in the Supporting Information.

The first notable structural feature of **8** is that it has a single magnetically distinct subunit (Figure 1A). This contrasts with dilithium salt **2**, which manifests two magnetically distinct subunits in equal (2:2) proportions. While not self-evident on simple inspection, prismatic core **5** observed for the dilithium salts requires two magnetically inequivalent subunits, suggesting that the disodium salt is fundamentally different. Second, there are two aging effects deriving from slow aggregate equilibrations, one quite subtle and of unknown consequence (discussed in the context of MCV below) and the other more striking and consequential.

In our first study of aging, samples of disodium enolate **8** were incrementally warmed and recooled. Subsequent ^{1}H and ^{13}C NMR spectra, recorded at −80 °C, showed no detectable structural changes after warming to −20 °C, at which point an irreversible change was observed (Figure 1). No further changes are noted on warming to >20 °C. Qualitatively, the spectral changes seemed to correlate with the emergence of aging effects that caused the reduced (20−50%) conversions in the alkylations. What is also notable from Figure 1C is that the new species appears to have two components in an approximate 3:1 ratio. We must confess, however, that the aging is erratic, varying considerably from sample to sample: Figure 1 is the cleanest example of this aging effect and has proven difficult to replicate. Systematic variations in the NaDA concentration suggest that aging is more acute at lower NaDA titers. Although the effect is real, we terminated efforts to understand it. Further hints, however, are discussed below.

The use of MCV[18] to determine the aggregation state of unaged samples involves making binary mixtures of structurally

DOI: 10.1021/jacs.9b08176
J. Am. Chem. Soc. XXXX, XXX, XXX−XXX

distinct enolates of unknown aggregation state, n, to generate an ensemble of homoaggregates ($\mathbf{A}_n$ and $\mathbf{B}_n$) and heteroaggregates ($\mathbf{A}_x\mathbf{B}_{n-x}$). The homo- and heteroaggregates could, in principle, be monitored using ^{1}H, ^{13}C, and ^{15}N NMR spectroscopies; ^{13}C{^{1}H} NMR spectroscopy sufficed for our purposes. The pairing partners must be sufficiently distinct to generate ensembles with adequate spectral resolution but similar enough to accurately reflect the aggregation states of the homoaggregates. We explored combinations of enolates **8** and **14**−**17** to generate homo- and heterochiral ensembles.

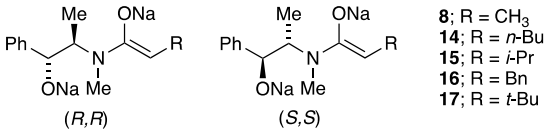

Before discussing the MCV results, we must briefly describe a second aging effect observable at −78 °C that would have gone undetected had we not undertaken the MCV studies. In short, we found that the method of enolization dictated the behavior of the ensemble (Scheme 1). Thus, the simultaneous addition

Scheme 1. Aging of Sodiated Enolate Mixtures

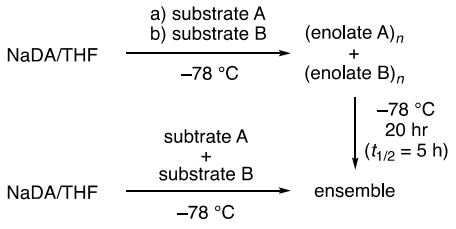

of both enolate precursors (substrate A + substrate B in THF) to NaDA to concurrently generate enolates **8** and **15** affords ensembles of homo- and heteroaggregates that outwardly appear normal (as exemplified in Figure 2). By contrast, the sequential addition of the enolate precursors to NaDA, with adequate delay to separate the enolizations and aggregations temporally, affords homoaggregates to the near exclusion of heteroaggregates. The two homoaggregates age to a fully equilibrated ensemble of homo- and heteroaggregates with an approximate half-life of 5 h at −78 °C. We have noted such aging effects for many enolates.[22] The time scale of this aging effect is distinctly different from that of the aging effect illustrated in Figure 1. We conclude that the concurrently generated enolates form ensembles of aggregates in rational proportions but under kinetic control. Accordingly, for the purposes of the MCV analysis, substrates were added concurrently, and the resulting ensembles were aged for 18−24 h at −78 °C to ensure full equilibration.

In the case of the octalithiated Myers enolates, heterochiral pairs of the same enolate, such as scalemic mixtures of (*R*,*R*)-**2** and (*S*,*S*)-**2**, gave us excellent resolution, yet afforded the wrong answer owing to a high thermochemical preference for 2:1 and 1:2 hexalithiated heterochiral forms.[5] To the best of our knowledge, that is a unique failure among hundreds of such MCV studies of lithium enolates. Mixtures of disodium salts (*R*,*R*)-**8** and (*S*,*S*)-**8**, by contrast, showed no evidence of heteroaggregation whatsoever. Fortunately, mixtures of **8** with structurally distinct enolates **14**−**17** in the homochiral (*R*,*R*) series worked well.

Binary mixtures generated from **8** and **14**−**17** form homochiral ensembles that are, without exception, consistent with a structural model showing octasodiated tetramers. The **8**−**15** pair with Me and *i*-Pr substituents, respectively (Figure 2), showed the best resolution. All ensembles showed homoaggregates manifesting a single magnetically distinct subunit as noted for **8**, a single isomeric form corresponding to 3:1 and 1:3 heteroaggregates, and two or three (out of a possible three) 2:2 heteroaggregates with the third isomer resolving reluctantly. These symmetries are important, vide infra. Plotting the relative concentrations of the homo- and heteroaggregates versus measured[23] mole fraction of dianionic subunit **15** (X_B) affords a Job plot fit to a tetramer-based model (Figure 3).

2D-NMR spectra recorded on unaged samples of **8** show a single magnetically discrete subunit (Figure 4). The phenyl

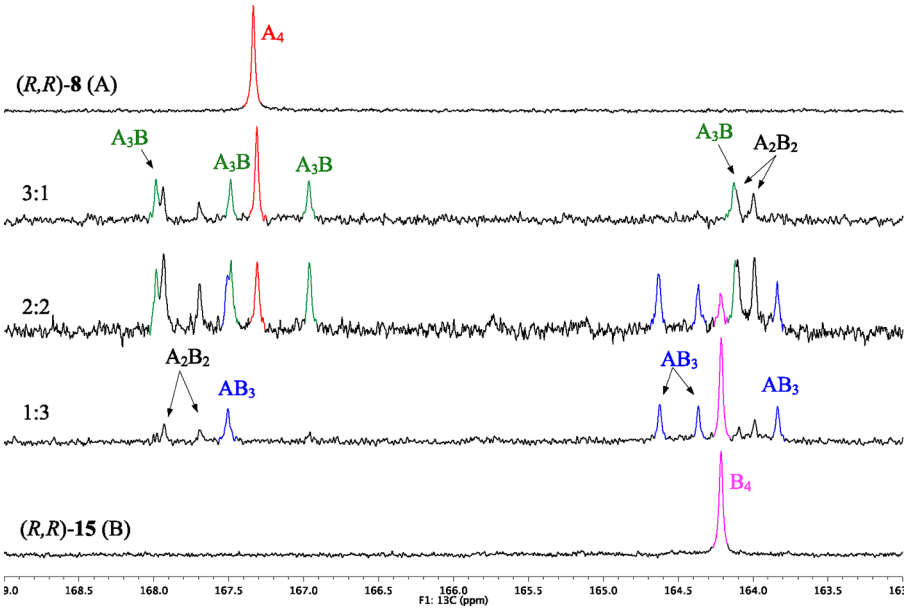

Figure 2. Partial ^{13}C{^{1}H} NMR spectra of solutions of disodium enolates (*R*,*R*)-**8** (A) and (*R*,*R*)-**15** (B; 0.25 M total concentration) in neat THF at −80 °C. Samples were maintained at −80 °C for 18−24 h to equilibrate the ensembles.

DOI: 10.1021/jacs.9b08176
J. Am. Chem. Soc. XXXX, XXX, XXX−XXX

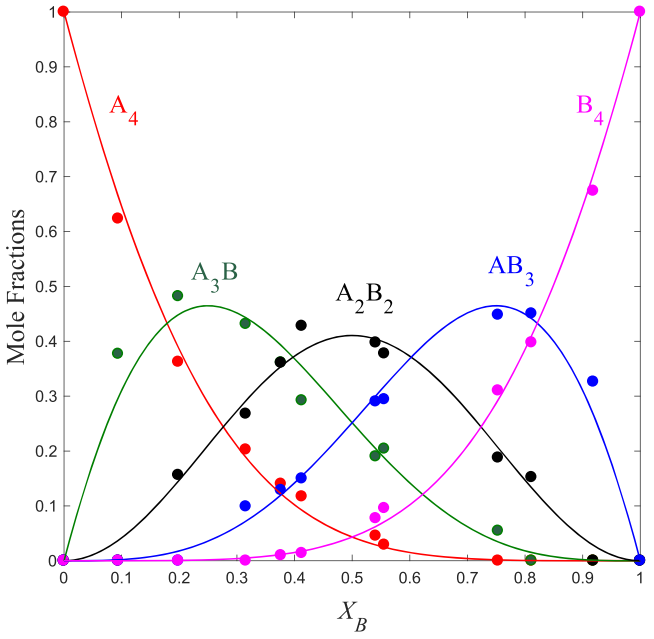

Figure 3. Job plot showing the relative integrations of octasodiated homoaggregates ($\mathbf{A_4}$ and $\mathbf{B_4}$) and heteroaggregates ($\mathbf{A_3B}$, $\mathbf{A_2B_2}$, and $\mathbf{AB_3}$) versus measured mole fractions[23] of (*R*,*R*)-**15** (X_B) for 0.25 M mixtures of sodium enolates (*R*,*R*)-**8** (**A**) and (*R*,*R*)-**15** (**B**) in neat THF at −80 °C. The curves result from a parametric fit to a tetramer model.[18b]

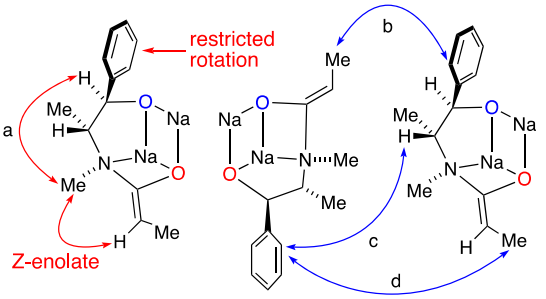

Figure 4. A single magnetically distinct subunit of **8** showing selected (important) intrasubunit correlations (red) and intersubunit correlations (blue).

moiety displays five discrete protons, indicating restricted rotation and evidencing low fluxionality. The Na−N contact shown in Figure 4 is reasonable based on analogous Li−N contacts in the dilithium salt **2**[5] and was supported both crystallographically and computationally (vide infra). The challenge with any homoaggregated species, however, is distinguishing between intra- and intersubunit correlations. Correlation "a" in Figure 4 suggests the phenyl resides on the concave face, but additional correlations, such as b−d, likely result from intersubunit contacts from proximate magnetically equivalent subunits. These ambiguities undermined our confidence in a structural assignment.

We resolved the ambiguity presented by intra- versus intersubunit correlations by leveraging the results from MCV. A 6:1 mixture of enolates **8** and **15** contained the homoaggregate of **8** along with low concentrations of a 3:1 heteroaggregate (**18**) with three magnetically inequivalent subunits of **8** and a single subunit of **15**. We successfully resolved significant portions of all four subunits in the 3:1 heteroaggregate (Supporting Information). The broken symmetry allowed us to show that the four magnetically distinct subunits contained phenyl moieties on the concave face, as drawn in Figure 4. The correlations (see Supporting Information) are fully consistent with 3:1 heteroaggregate **18** (Figure 5), which, in turn, supported the assignment of the homoaggregate of **8** as homotetramer **19**.

The octagonal prismatic structure of **19** with four THF ligands coordinated to the sodiums that do not have Na−N contacts was computationally viable. If, however, four THF ligands are placed on the proximal sodiums to generate a tetrasolvate with N−Na−THF connectivity, the aggregate collapses to stacked cube (**20**, Figure 5).[24] Although it seems less intuitive (to us at least) to solvate the sodium already bearing a nitrogen-based ligand, **20** is calculated to be 13 kcal/mol more stable than **19**. Aggregate **20** shows the same symmetry and is fully consistent with the spectroscopic data. Although we do not view the computations as the definitive answer, we will refer to the tetramer as **20** from this point forward.

A potential alternative homotetramer, **21**, displays the same high symmetry as **20** and is computationally preferred by 3 kcal/mol relative to **20**. In contrast to **20** with the enolate oxygens on the top and bottom faces of the stack, stacked cube **21** places the enolate oxygens in the internal positions. However, **21** (as well as the corresponding octagonal prismatic form) is missing critical spatial relationships observed spectroscopically.

X-ray Structure of Decomposition. A crystal grown by fully aging a sample of enolate **8** at ambient temperatures afforded the X-ray crystal structure of aggregate **22** shown in Figure 6. Although the crystal structure of **22** is not what a crystallographer would call publishable and offers no insights into the solution structure of **8** in unaged samples, it does contain several notable features. The aggregate is composed of six dianionic subunits of **8** and two monoanionic alkoxides (**23**) resulting from protonation of the enolate. The structure shows a number of Na−N contacts akin to the Li−N contacts noted for enolate **2** and supported computationally in Figure 6.

The structure in Figure 6 seemed spurious (a rogue) on first inspection. Recall, however, that a warming solution of enolate **8** generates (albeit irreproducibly) a new species with resonances in a 3:1 ratio (Figure 1C), as would be expected for **22**, and that alkylations of such aged samples suffer from significantly reduced percent conversions (50−80%). Aggregate **22** and related decompositions occur in sealed tubes containing no obvious proton source. Is it possible that aggregate **20** scavenges 2 equiv of diisopropylamine to regenerate NaDA (eq 4)? We are untroubled by the thermochemistry implicit in eq 4, given that aggregate-based stabilizations can be considerable. This hypothesized proton transfer from *i*-Pr_2NH is vaguely reminiscent of deuteration studies in which Seebach was forced to invoke transitory proton transfers from the *i*-Pr_2NH to an enolate to explain failed deuterations.[25] One control experiment supports this hypothesis. Deuteration of an unaged sample of **8** with MeOD afforded 95% of the expected monodeuterated **1**. By contrast, a parallel sample of **8**, prepared from the same stock solutions, was aged for 90 min at 25 °C, and then quenched with MeOD. In this reaction, **1** was recovered cleanly but with only <10% deuteration.

$$\mathbf{20} + 2i\text{-}Pr_2NH \rightarrow \mathbf{22} + 2\text{NaDA} \quad (4)$$

Aging Effects: Lingering Concerns. Qualitatively, the aging effects on structure correlate with reduced conversions in

DOI: 10.1021/jacs.9b08176
J. Am. Chem. Soc. XXXX, XXX, XXX−XXX

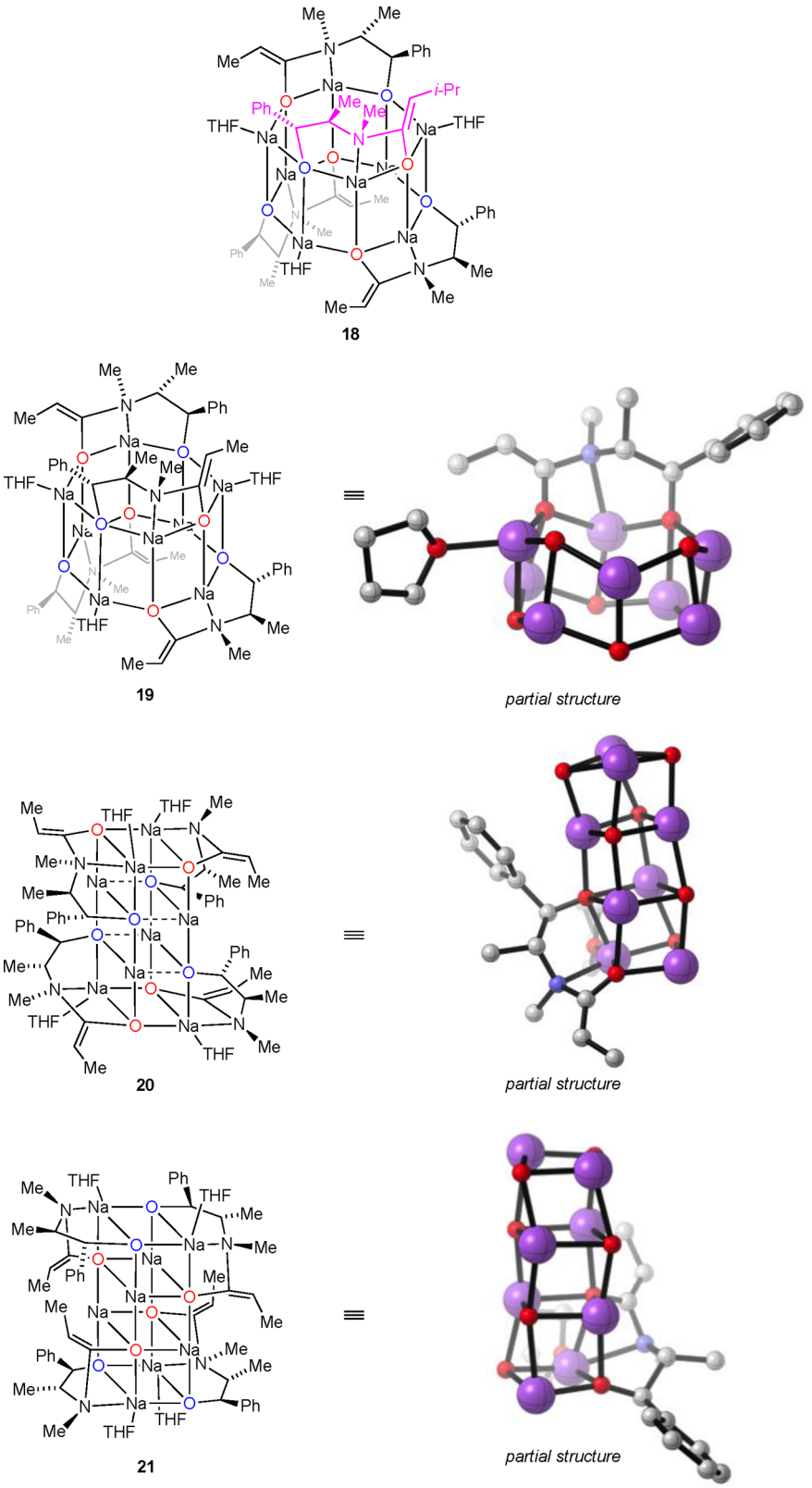

Figure 5. Tetrameric aggregates of Myers enolates and partial structures of the computed forms.

the alkylation of enolate **8**. Quantitatively, the alkylation seems to be more sensitive to temperature than are the spectroscopically studied aggregate exchanges. We suspect that this discrepancy arises from aging effects on the mixed aggregates formed at partial conversion. This is a difficult assertion to document. The fact that warming causes inferior alkylation also suggests that aging is more temperature sensitive than is the alkylation. A second quantitative discord comes from rate studies (below) showing reversible deaggregation that seems more facile than the formation of heteroaggregates in Scheme 1.

DOI: 10.1021/jacs.9b08176
J. Am. Chem. Soc. XXXX, XXX, XXX−XXX

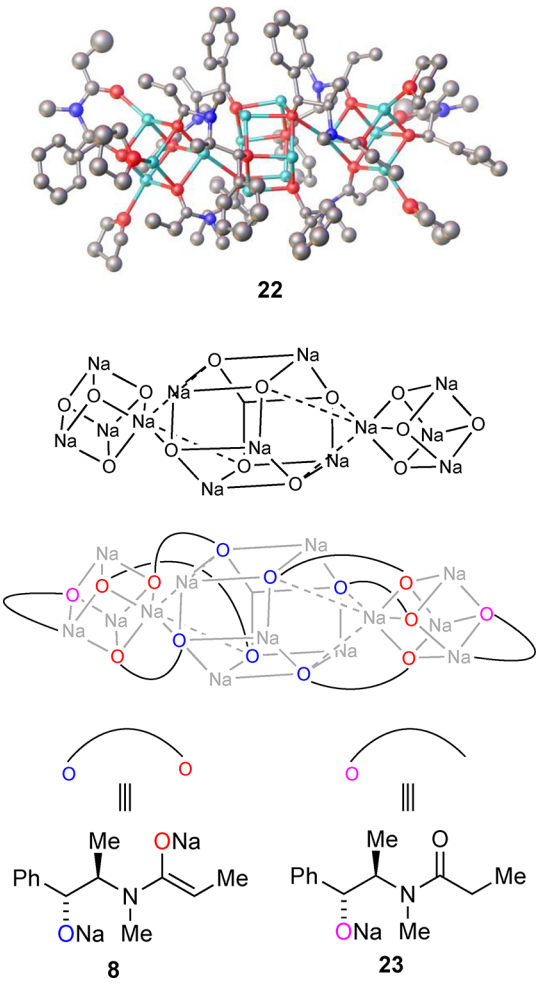

Figure 6. X-ray structure of **22** containing six dianions corresponding to **8** and two alkoxides corresponding to **23**. THFs are omitted for clarity.

In this case, reduced dissociation rates of the more sterically demanding **15** would inhibit exchange with **8**. We were unable to design a satisfying experiment to investigate the intersubunit exchange using only enolate **8**.

Rate Studies and Mechanism. Monitoring the alkylation of 0.10 M **8** with 0.40 M *n*-BuI in neat THF-d_8 by ^{1}H NMR spectroscopy shows an initial burst of 1-butene owing to instantaneous E2-elimination by the slight excess of NaDA, which confirms adequate titer and serves as an internal standard. The slow loss of **8** (aggregate **20**) and formation of new products (Figure 7) is surprisingly clean given how complex the spectra could have been owing to intervening mixed aggregates. Although we suspected the new species may be the alkoxide of product **9** (R = *n*-Bu), metalation of **9** with 1.0 equiv of NaDA to generate an authentic sample afforded complex resonances. (Of course, such control experiments are difficult to interpret without understanding the aging of the alkoxide.) Plotting the disappearance of tetramer **20** over time reveals a decay that, while necessarily neither first nor second order (Figure 8), shows no significant evidence of autoinhibition or autocatalysis. Alkylations of samples spiked with highly soluble NaI show no measurable rate effects. In theory, tetramer **20** could be fully consumed at low (25%) conversion and replaced by new, altogether different mixed aggregates retaining multiple dianionic and monoanionic subunits. In practice, quenching samples shows that percent conversion in the crude product correlates with the spectroscopic loss of **20**.

Rate studies using the method of initial rates[26] show a first-order dependence on *n*-BuI (Figure 9), a third-order dependence on THF (Figure 10), and, most critically, a 1/4-order dependence on aggregate **20** (Figure 11).[27] The natural log version of Figure 11 is included as an inset.[28] The idealized rate law[29] in eq 5 is consistent with the generic mechanism in eqs 6 and 7.[30] The mechanism presumes that tetramer **20** has one coordinated THF ligand per subunit, an assumption with computational but no experimental support.

$$-\mathrm{d}[\mathbf{20}]/\mathrm{d}t = k[\mathbf{20}]^{1/4}[n\text{-BuI}][\mathrm{THF}]^3 \tag{5}$$

$$\underset{\mathbf{20}}{\frac{1}{4}(\mathrm{enolate})_4(\mathrm{THF})_4} + 3\mathrm{THF} \rightleftharpoons \mathrm{enolate}(\mathrm{THF})_4 \tag{6}$$

$$\mathrm{enolate}(\mathrm{THF})_4 + n\text{-BuI} \rightarrow \frac{1}{x}(\mathrm{RONa})_x + \mathrm{NaI} \tag{7}$$

Although tetramer **20** foreshadows potential structural details of a fleeting monomeric intermediate, the similarities would be superficial. The resting state of the tetrasolvated monomers, however, should share many structural features with the rate- and product-determining transition structures. Figure 12 shows the two most stable tetrasolvated monomers, **24** and **25**, of eight total. Before discussing the three critical variables that required careful evaluation, we should mention a few that are non-negotiable because only one option is viable.

Without fail, all eight computed tetrasolvated monomers show an irresistible penchant to form a tight Na–N contact (2.4–2.5 Å). An analogous contact was observed in the lithium variants and is observed in crystal structures of simple lithium carboxamide enolates by Williard and co-workers.[31] A THF bridging the sodium cations shown in Figure 12 was also computationally unavoidable. Such bridging THFs are documented crystallographically for both sodium[32] and lithium.[33] We have also invoked them as potentially important fleeting intermediates in deaggregations.[34] The three η^1-bound (terminal) THF ligands are decidedly tetrahedral at oxygen, unlike the trigonal planar geometries of lithium-bound THFs. This differential preference was noted decades ago by Seebach and Dunitz from a survey of the crystallographic database.[35]

The three important variables demanding our full attention are as follows. First, a simple chair–chair flip interconverts pseudodiequatorial substituents along the ethanolamine backbone with an Ar–C–C–Me torsional angle of 44–57° (see **24**) to a pseudodiaxial form with a torsional angle of 159–172° (see **25**). Next, the phenyl moiety can reside either on the concave (endo) face as in **24** or on the convex (exo) face as in **25**. (As an aside, the phenyl on the concave face is preferred in tetramer **20**.) Last, the fourth THF can be placed either proximate to the N–bound sodium (not shown) or on the seemingly more open sodium, as shown in both **24** and **25**. Oddly, these two most stable structures share only one of three variables, the THF placement. Even then, other reasonable structures have the alternative placement. The eight isomers span a 9–10 kcal/mol range.

Of course, the selectivities are dictated by the competing transition states (modeled with EtBr). The transition states are subject to all of the vicissitudes found in the monomeric resting states discussed above and several unique to the transition structures. The orientation of the methyl moiety of EtBr is non-

DOI: 10.1021/jacs.9b08176
J. Am. Chem. Soc. XXXX, XXX, XXX–XXX

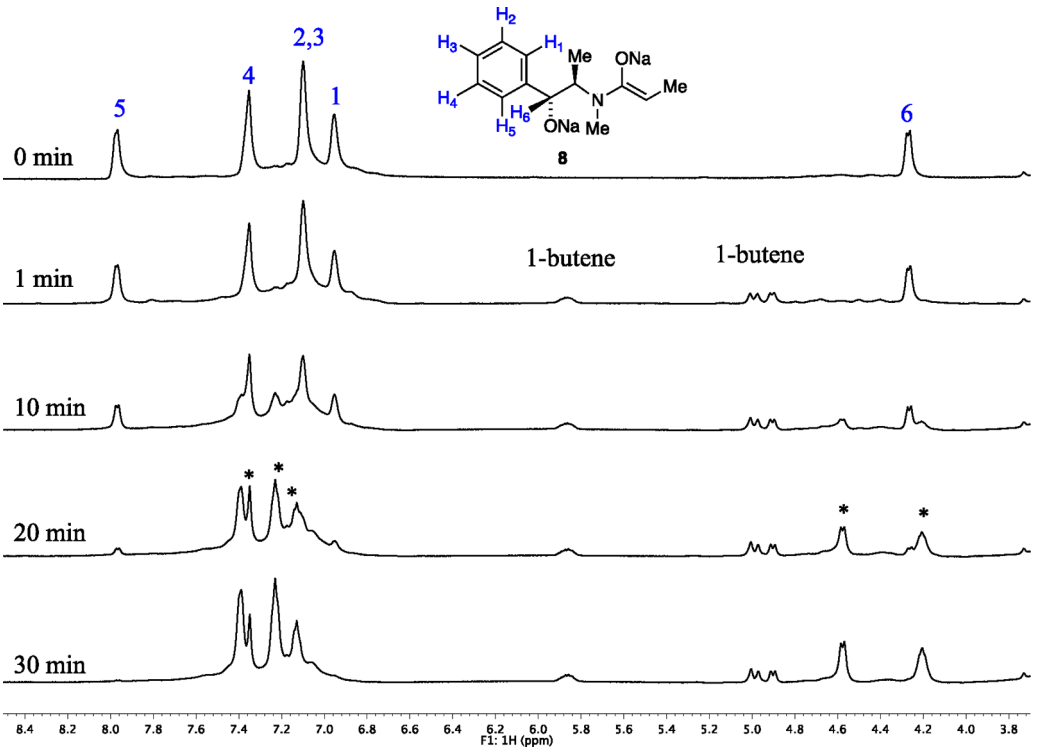

Figure 7. ^{1}H NMR spectra following the alkylation of **8** (0.10 M) with *n*-BuI (0.40 M) in neat THF-d_8 at −60 °C with formation of an uncharacterized product (*).

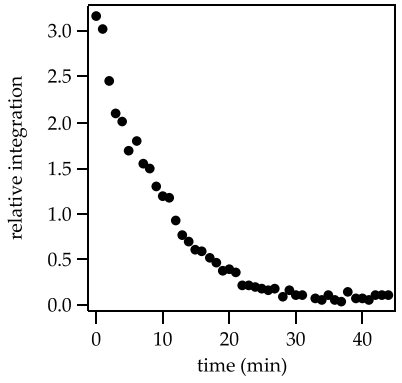

Figure 8. Decay of dianion **8** (0.10 M) with *n*-BuI (0.40 M) in neat THF-d_8 at −60 °C as shown in Figure 7.

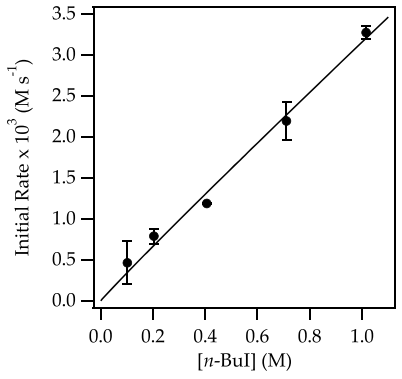

Figure 9. Plot of initial rate versus *n*-BuI concentration for alkylation of 0.10 M **8** in neat THF-d_8 at −80 °C. The curve depicts an unweighted least-squares fit to the function $f(x) = ax^n$ such that $a = (3 \pm 1) \times 10^{-3}$, $n = 0.97 \pm 0.08$.

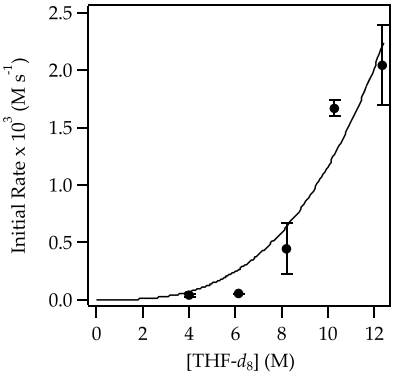

Figure 10. Plot of initial rate versus THF-d_8 concentration for alkylation of 0.050 M **8** and 0.20 M *n*-BuI in hexanes cosolvent at −80 °C. The curve depicts an unweighted least-squares fit to the function $f(x) = ax^n$ such that $a = (1 \pm 2) \times 10^{-6}$, $n = 3.0 \pm 0.9$.

negotiable; one rotamer is markedly preferred over the other two. The EtBr can approach the concave (endo) or convex (exo) face but invariably with Na−Br contacts. Exo approach is accompanied by a Na−Br contact proximate to the Na−N contact, whereas endo approach shows a Na−Br contact on the sodium distal to the nitrogen. Figure 13 illustrates the two lowest energy transition structures (of 16 total) leading to the major product (**26**) and minor product (**27**). The other 14 transition structures have been archived in the Supporting Information. Transition structures **26** and **27** also correspond to approach of the EtBr to the *endo* and *exo* faces, respectively. Intrinsic reaction coordinate (IRC) calculations[36] on **26** and **27** afford first-formed minima with marked lengthening of the Na−N bonds and only marginal additional shortening of the Na−Br bonds.

DOI: 10.1021/jacs.9b08176
J. Am. Chem. Soc. XXXX, XXX, XXX−XXX

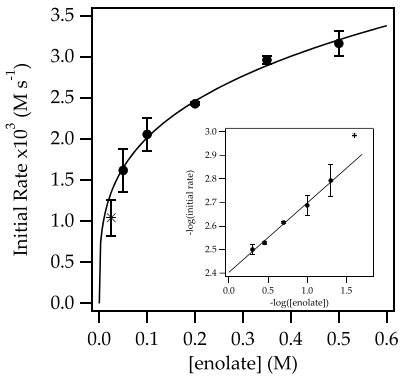

Figure 11. Plot of initial rate versus enolate **8** concentration for alkylation of **8** with 0.49 M *n*-BuI in neat THF-d_8 at −80 °C. The asterisk (*) denotes a point at 0.025 M enolate in which poor signal-to-noise rendered it unreliable. The curve depicts an unweighted least-squares fit to the function $f(x) = ax^n$ such that $a = (3.9 \pm 0.1) \times 10^{-3}$, $n = 0.29 \pm 0.01$. The inset shows the log(initial rate) versus log[enolate]. The curve depicts an unweighted least-squares fit to the function $f(x) = ax+b$ such that $a = 2.40 \pm 0.01$, $b = 0.29 \pm 0.01$.

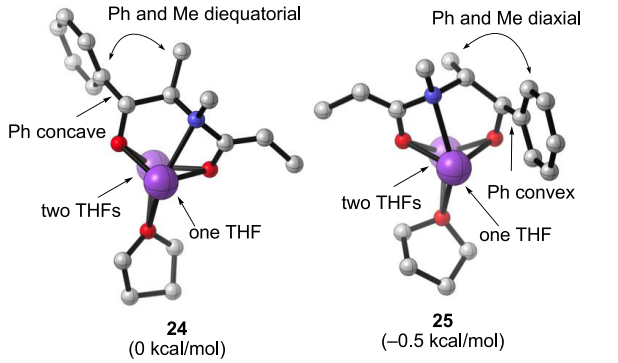

Figure 12. Two most stable resting states for tetrasolvated monomeric enolate **8** with relative energies. η^1 THFs are omitted for clarity.

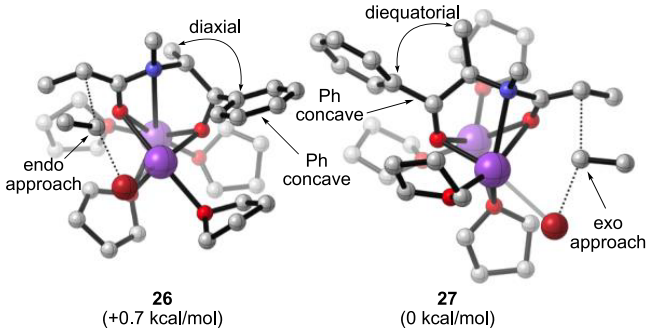

Figure 13. Two most stable transition structures for tetrasolvated monomer-based alkylations with ethyl bromide leading to the experimentally observed major product (**26**) and minor product (**27**) with relative energies.

Transition structures **26** and **27** in Figure 13 include one more niggling detail: they predict the wrong stereochemistry by 0.7 kcal/mol. This is not a shocking failure and could be argued to be within the propagated error of the calculations given the number of variables involved. Probes for potential problems included single point calculations on **26** and **27** with the η^1-bound THFs removed or with the methyls and phenyls along the ethanolamine backbone replaced by 1.11 Å C−H bonds. Neither probe revealed an obvious source of the failed prediction. Examining other basis sets similarly afforded no consequential differences, only interesting philosophical questions discussed below. We even considered the possibility that the THF order in Figure 10 is misleading and probed the trisolvated monomers (Supporting Information), but they offered no relief from the cunundrum.

Largely for entertainment value, we created a composite of the ideal transition state by averaging the contributions of the four variables independently. The 16 transition states offer four sets of eight binary pairs in which only one variable has been changed. Accordingly, on average the preferred orientations include pseudodiequatorial substituents on the ethanolamine backbone (−1.2 ± 4.3 kcal/mol), disolvation distal from the Na−N contact (−1.2 ± 4.4 kcal/mol), placement of the phenyl moiety on the convex face and methyl on the concave face (−0.8 ± 2.4 kcal/mol), and exo approach of EtBr (−0.6 ± 5.9 kcal/mol). The near thermoneutral preferences and large error bars aside, this statistical composite (**28**, Figure 14) with each

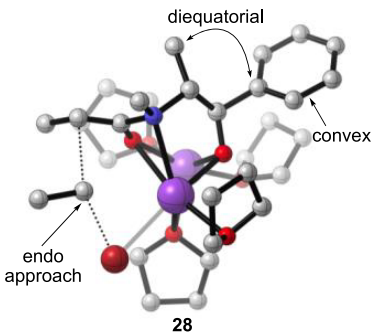

Figure 14. Statistical composite transition structure **28** defined by control of four key variables in their preferred modes.

variable in the preferred orientation, while not the most stable transition structure of the 16 transition structures considered, predicts the major alkylation product. This thought experiment is provocative but should not be taken too seriously.

The above discussion underscores some deeply philosophical issues. Several decades of exploring computational chemistry within the confines of organolithium chemistry have revealed many details that we were not savvy enough to anticipate. Such computational discoveries forcibly remove some human bias. Bridging THF ligands and Li−N/Na−N contacts foisted upon us during studies of Myers enolates are emblematic. Suppose, however, that shopping for basis sets had revealed one that replicated the selectivity that we already knew from experiment. Should we simply use that basis set? Is this really proper scientific method? In the isolated world of one case study and from investigators who are, relatively speaking, Luddites computationally, we do not think so. Such an observation would, however, prompt us to try that basis set again in future case studies. Should superior experiment−theory correlations from that basis set persist, then the beginnings of an important trend have emerged.

The synergies of experimental and computational data are critical. By using both, we are examining the efficacy of the computations as much as computationally probing structure and mechanism. Failed theory−experiment correlations prompt us to question both the theory and the experiment. Is it a problem with the basis set, the THF order, or user error? One should not underestimate the sensitivity of the computational results to the user's willingness to probe alternatives and the

DOI: 10.1021/jacs.9b08176
J. Am. Chem. Soc. XXXX, XXX, XXX−XXX

incursion of confirmation bias. We wonder whether computational data in the absence of supporting mechanistic data should be referred to as elucidating a mechanism or merely examining it. With that said, we submit that as the computational community improves its methods, the broader organic chemistry community benefits from bringing computations to bear on experimental problems, even if these computations are not done with the greatest skill or attention to detail. They should be allowed to do so without fear of falling short of the state-of-the-art standards. It has been said by physician Howard Skipper that "a model is a lie that helps you see the truth."

CONCLUSIONS

The alkylations of disodiated Myers enolates provide results that are largely comparable to those obtained by Myers using dilithiated enolate **2**/LiCl mixtures. The disodium salts have the advantage that they do not require additives and, consequently, can be effected at high concentrations preferred for industrial scales. There are, however, offsetting costs. Alkylations of the disodium salts require more rigorous temperature control to prevent aging and O-alkylations, and several electrophiles simply did not react well.

The aging effects remind us that many who use enolates likely do not understand how robust enolate aggregates can be. Aggregate exchanges can be so slow that equilibration requires warming to ambient temperatures.[22] Any effort to optimize the chemistry of alkali metal enolates must respect the complexity that this phenomenon imposes. In a study reported two decades ago, Merck investigators found that an aging step was critical to success.[37] Myers bypassed a highly problematic aging by adding 5 equiv of LiCl, but even then, the procedure required warming to ambient temperatures to form the requisite dilithiated enolate−LiCl adduct. In the case of disodium Myers enolates, aging is a destructive process in which the enolization appears to be pushed in reverse to produce unenolized alkoxide. Of course, every enolate−solvent combination is unique, but it seems likely that synthetic chemists are getting whipsawed by such aging effects without realizing it.

The results of the disodium salt alkylations cause us to reflect on the mechanistic studies of the dilithium Myers enolates. Our failure to assign the structure of the key LiCl adduct of enolate **8** left us with three mechanistic possibilities, including one in which the LiCl adduct was suggested to be a fluctional source of the LiCl-free monomer. Given the monomer-based alkylation of the disodium salt, the analogous monomer-based mechanism for the dilithium salt gains credibility. Some of the details of the computational data from that study show parallels, including a Li−Br contact and bridging THF.[5]

Going forward, several issues remain to be resolved. The obvious next move is to explore both dilithium and disodium salts of the diphenyl-substituted second-generation enolates derived from **3**. It should be much easier now. Taking a more expanded view, the protocols to probe Myers enolates should translate to other synthetically important dianions used routinely in organic synthesis.[17,38] Last, unraveling the structure−reactivity relationships of disodium Myers enolates represents progress toward understanding and further developing organosodium chemistry to pique the interest of those who use alkali metal-based reagents.

EXPERIMENTAL SECTION

Reagents and Solvents. THF and hexane were distilled from solutions containing sodium benzophenone ketyl. NaDA used for structural and mechanistic studies was prepared as a white crystalline solid as described previously[11a] and manipulated using a standard glovebox, vacuum line, and syringe techniques. The benchtop procedures used no specialized inert atmosphere equipment as described below. Myers enolate precursors were either purchased or prepared as described previously.[1]

NMR Spectroscopy. Stock solutions of NaDA/THF were prepared at −78 °C and held at this temperature until spectra were recorded. An NMR tube under vacuum was flame-dried on a Schlenk line and allowed to return to room temperature. It was then backfilled with argon and placed in a dry ice/acetone bath at −78 °C. The appropriate amounts of acylated pseudoephedrine and NaDA (2.5 equiv) were added sequentially via syringe. The tube was sealed under partial vacuum and vortexed three times on a vortex mixer for 5 s. Samples could be stored for up to 2 weeks in a freezer at −86 °C. Each sample typically contained 0.25 M total enolate titer generated using 0.63 M NaDA (0.13 M excess). Standard ^{1}H and ^{13}C NMR spectra were recorded on a 500 MHz spectrometer at 499.92 and 73.57 MHz, respectively. ^{13}C resonances are referenced to the CH_2O resonance of THF at −80 °C (67.57 ppm). Two-dimensional NMR spectroscopies (COSY, HMBC, HSQC, NOESY, and ROESY) were recorded using standard pulse sequences.

IR Spectroscopic Analyses. IR spectra were recorded using an in situ IR spectrometer fitted with a 30-bounce, silicon-tipped probe. The spectra were acquired in 16 scans at a gain of 1 and a resolution of 4 cm^{-1}. A representative reaction was carried out as follows: The IR probe was inserted through a nylon adapter and O-ring seal into an oven-dried, cylindrical flask fitted with a magnetic stir bar and a T-joint. The T-joint was capped with a septum for injections and a nitrogen line. After evacuation under full vacuum, heating, and flushing with nitrogen, the flask was charged with a stock solution of enolate **8** in neat THF. The vessel was cooled to −78 °C in a dry ice bath prepared using fresh acetone. After a background spectrum was recorded, neat alkyl halide was added with stirring. IR spectra were recorded every 6 s with monitoring of the absorbance at 1620 cm^{-1} over the course of the reaction.

MCV. The mathematical treatment for creating Job plots using Matlab has been described in detail previously.[18b]

Representative NaDA Preparation. Sodium slices (600 mg) cut from sodium cubes were placed in a 50 mL pear-shaped flask. Dry THF (5.0 mL) and technical-grade diisopropylamine (3.0 mL, 21 mmol) were added to the flask under positive argon pressure, and the mixture was maintained at 20 °C. Isoprene (1.0 mL, 10 mmol) was added at 0 °C all at once. Stirring for 45 min yielded a brown-yellow solution. Darkening of the sodium surface appears to correlate with the completion of the reaction. The solution is readily decanted by syringe from with unreacted sodium slices and should be done so promptly (<2 h) to prevent gelling. The resulting yellow-brown solution should be used within 5 h if stored at 0 °C or within 48 h if stored at −20 °C. (Warming to 0 °C makes handling the viscous solution easier.) Titration[15] routinely affords 80−90% of the anticipated normality (1.6−1.8 M). A 10-fold scale-up (200 mmol) afforded analogous results without a measurable exotherm. Monitoring the internal reaction temperatures on larger scale reactions is advised. The spent sodium is quenched by adding sequentially adding hexane followed by isopropanol dropwise.

Representative Alkylation with *n*-BuI. 100 mg (0.45 mmol) of **1** was added to a flame-dried 5 mL pear shaped flask equipped with a T-joint and a magnetic stir bar under argon and cooled to −78 °C. NaDA in THF solution (800 μL, 1.41 M, 1.13 mmol) was added. The mixture was stirred at −78 °C for 20 min until substrate **1** dissolved. *n*-BuI (100 μL, 0.87 mmol, 1.9 equiv) was added to the solution and stirred at −78 °C for 6 h (or −40 °C for 1 h). The reaction was quenched with saturated NH_4Cl (0.50 mL), and the resulting biphasic mixture was partitioned between water (0.50 mL) and ethyl acetate (10 mL). The aqueous layer was separated and extracted further with three 5 mL portions of ethyl acetate. The combined organic layers were dried over anhydrous magnesium sulfate, filtered, and then concentrated. Purification of the residue by flash column chromatography (50% ethyl acetate in hexanes) afforded 103 mg (82%) of

DOI: 10.1021/jacs.9b08176
J. Am. Chem. Soc. XXXX, XXX, XXX−XXX

product as a white crystalline solid whose spectral properties were found to be in accordance with those previously reported.[1a]

Representative Kinetic Reaction. A representative reaction was carried out as follows: an NMR tube equipped with double septa was charged with 0.15 M **1** in THF-d_8 (400 μL) and 0.75 M NaDA in THF-d_8 (200 μL). The sample was vortexed three times on a vortex mixer for 5 s with cooling between each vortexing. To this solution was added *n*-BuI. ^{1}H NMR spectra were recorded at −80 °C at 1.0 min intervals.

■ ASSOCIATED CONTENT

Supporting Information

The Supporting Information is available free of charge on the ACS Publications website at DOI: 10.1021/jacs.9b08176.

Spectroscopic, crystallographic, computational, rate, and MCV data (PDF)

■ AUTHOR INFORMATION

Corresponding Author

*dbc6@cornell.edu

ORCID

Samantha N. MacMillan: 0000-0001-6516-1823

David B. Collum: 0000-0001-6065-1655

Notes

The authors declare no competing financial interest.

■ ACKNOWLEDGMENTS

We thank the National Institutes of Health (GM131713) for support.

■ REFERENCES

(1) (a) Myers, A. G.; Yang, B. H.; Chen, H.; Gleason, J. L. Use of Pseudoephedrine as a Practical Chiral Auxiliary for Asymmetric Synthesis. *J. Am. Chem. Soc.* **1994**, *116*, 9361. (b) Myers, A. G.; McKinstry, L. Practical Syntheses of Enantiomerically Enriched γ-Lactones and γ-Hydroxy Ketones by the Alkylation of Pseudoephedrine Amides with Epoxides and their Derivatives. *J. Org. Chem.* **1996**, *61*, 2428. (c) Myers, A. G.; Yang, B. H.; Chen, H.; McKinstry, L.; Kopecky, D. J.; Gleason, J. L. Pseudoephedrine as a Practical Chiral Auxiliary for the Synthesis of Highly Enantiomerically Enriched Carboxylic Acids, Alcohols, Aldehydes, and Ketones. *J. Am. Chem. Soc.* **1997**, *119*, 6496.

(2) Evans, D. A.; Takacs, J. M. Enantioselective Alkylation of Chiral Enolates. *Tetrahedron Lett.* **1980**, *21*, 4233.

(3) (a) Mellem, K. T.; Myers, A. G. A Simple, Scalable Synthetic Route to (+)- and (−)-Pseudoephenamine. *Org. Lett.* **2013**, *15*, 5594. (b) Morales, M. R.; Mellem, K. T.; Myers, A. G. Pseudoephenamine: A Practical Chiral Auxiliary for Asymmetric Synthesis. *Angew. Chem., Int. Ed.* **2012**, *51*, 4568. (c) Hogan, P. C.; Chen, C.-L.; Mulvihill, K. M.; Lawrence, J. F.; Moorhead, E.; Rickmeier, J.; Myers, A. G. Large-scale Preparation of Key Building Blocks for the Manufacture of Fully Synthetic Macrolide Antibiotics. *J. Antibiot.* **2018**, *71*, 318.

(4) (a) Sandham, D. A.; Taylor, R. J.; Carey, J. S.; Fässler, A. A Convergent Synthesis of the Renin Inhibitor CGP60536B. *Tetrahedron Lett.* **2000**, *41*, 10091. (b) Dragovich, P. S.; Prins, T. J.; Zhou, R. Formal, Stereoselective Synthesis of Hydroxyethylene Dipeptide Isosteres Utilizing Pseudoephedrine Amides. *J. Org. Chem.* **1997**, *62*, 7872. (c) Sinz, C.; Bittner, A.; Brady, E.; Candelore, M.; Dallas-Yang, Q.; Ding, V.; Jiang, G.; Lin, Z.; Qureshi, S.; Salituro, G.; Saperstein, R. Discovery of *N*-Aryl-2-Acylindole Human Glucagon Receptor Antagonists. *Bioorg. Med. Chem. Lett.* **2011**, *21*, 7124. (d) Narasimhulu, C. P.; Das, P. Stereoselective Preparation of C1-C10 and C11-O14 Fragments of Narbonolide: Exploiting the Versatility of Thiazolidinethione Chiral Auxiliary. *Synthesis* **2009**, *2009*, 474.

(5) Zhou, Y.; Jermaks, J.; Keresztes, I.; MacMillan, S. N.; Collum, D. B. Pseudoephedrine-Derived Myers Enolates: Structures and Influence of Lithium Chloride on Reactivity and Mechanism. *J. Am. Chem. Soc.* **2019**, *141*, 5444.

(6) Johnson, N. W. Convex Solids with Regular Faces. *Can. J. Math.* **1966**, *18*, 169.

(7) Investigators at Merck carried out a facile Michael addition to a highly stabilized arene-substituted Myers dianion generated using LiHMDS in TMEDA/THF without added lithium salts. Added LiCl reverses the stereoselectivity. (a) Smitrovich, J. H.; Boice, G. N.; Qu, C.; DiMichele, L.; Nelson, T. D.; Huffman, M. A.; Murry, J.; McNamara, J.; Reider, P. J. Pseudoephedrine as a Chiral Auxiliary for Asymmetric Michael Reactions: Synthesis of 3-Aryl-δ-lactones. *Org. Lett.* **2002**, *4*, 1963. (b) Smitrovich, J. H.; DiMichele, L.; Qu, C.; Boice, G. N.; Nelson, T. D.; Huffman, M. A.; Murry, J. Michael Reactions of Pseudoephedrine Amide Enolates: Effect of LiCl on Syn/Anti Selectivity. *J. Org. Chem.* **2004**, *69*, 1903.

(8) Sarabu, R.; Bizzarro, F. T.; Corbett, W. L.; Dvorozniak, M. T.; Geng, W.; Grippo, J. F.; Haynes, N.-E.; Hutchings, S.; Garofalo, L.; Guertin, K. R.; Hilliard, D. W.; Kabat, M.; Kester, R. F.; Ka, W.; Liang, A.; Mahaney, P. E.; Marcus, L.; Matschinsky, F. M.; Moore, D.; Racha, J.; Radinov, R.; Ren, Y.; Qi, L.; Pignatello, M.; Spence, C. L.; Steele, T.; Tengi, J.; Grimsby, J. Discovery of Piragliatin—First Glucokinase Activator Studied in Type 2 Diabetic Patients. *J. Med. Chem.* **2012**, *55*, 7021.

(9) (a) Seebach, D. Structure and Reactivity of Lithium Enolates. From Pinacolone to Selective C-Alkylations of Peptides. Difficulties and Opportunities Afforded by Complex Structures. *Angew. Chem., Int. Ed. Engl.* **1988**, *27*, 1624. (b) Braun, M. Lithium Enolates: 'Capricious' Structures - Reliable Reagents for Synthesis. *Helv. Chim. Acta* **2015**, *98*, 1.

(10) Leading references to organosodium chemistry: (a) Mulvey, R. E.; Robertson, S. D. Synthetically Important Alkali-Metal Utility Amides: Lithium, Sodium, and Potassium Hexamethyldisilazides, Diisopropylamides, and Tetramethylpiperidides. *Angew. Chem., Int. Ed.* **2013**, *52*, 11470. (b) Seyferth, D. Alkyl and Aryl Derivatives of the Alkali Metals: Useful Synthetic Reagents as Strong Bases and Potent Nucleophiles. 1. Conversion of Organic Halides to Organoalkali-Metal Compounds. *Organometallics* **2006**, *25*, 2. (c) Seyferth, D. Alkyl and Aryl Derivatives of the Alkali Metals: Strong Bases and Reactive Nucleophiles. 2. Wilhelm Schlenk's Organoalkali-Metal Chemistry. The Metal Displacement and the Transmetalation Reactions. Metalation of Weakly Acidic Hydrocarbons. Superbases. *Organometallics* **2009**, *28*, 2. (d) Benkeser, R. A.; Foster, D. J.; Sauve, D. M.; Nobis, J. F. Metalations With Organosodium Compounds. *Chem. Rev.* **1957**, *57*, 867.

(11) (a) Ma, Y.; Algera, R. F.; Collum, D. B. Sodium Diisopropylamide in *N,N*-Dimethylethylamine: Reactivity, Selectivity, and Synthetic Utility. *J. Org. Chem.* **2016**, *81*, 11312. (b) Algera, R. F.; Ma, Y.; Collum, D. B. Sodium Diisopropylamide: Aggregation, Solvation, and Stability. *J. Am. Chem. Soc.* **2017**, *139*, 7921. (c) Ma, Y.; Algera, R. F.; Woltornist, R. A.; Collum, D. B. Sodium Diisopropylamide-Mediated Dehydrohalogenations: Influence of Primary- and Secondary-Shell Solvation. *J. Org. Chem.* **2019**, *84*, ASAP.

(12) Barr, D.; Dawson, A. J.; Wakefield, B. J. A Simple, High-Yielding Preparation of Sodium Diisopropylamide and Other Sodium Dialkylamides. *J. Chem. Soc., Chem. Commun.* **1992**, 204.

(13) (a) Lochmann, L.; Pospíšil, J.; Lím, D. On the Interaction of Organolithium Compounds with Sodium and Potassium Alkoxides. A New Method for the Synthesis of Organosodium and Organopotassium Compounds. *Tetrahedron Lett.* **1966**, *7*, 257. (b) Lochmann, L.; Janata, M. 50 Years of Superbases Made from Organolithium Compounds and Heavier Alkali Metal Alkoxides. *Cent. Eur. J. Chem.* **2014**, *12*, 537. (c) Lochmann, L.; Trekoval, J. Interactions of Alkoxides: XI. Reactions of Substituted *N*-Lithium Amides with Heavier Alkali Metal Alkoxides. a Novel Method for the Preparation of *N*-Sodium and *N*-Potassium Dialkylamides. *J. Organomet. Chem.* **1979**, *179*, 123.

DOI: 10.1021/jacs.9b08176
J. Am. Chem. Soc. XXXX, XXX, XXX−XXX

(14) Because of the second-order THF dependence and one-half-order NaDA dependence on the NaDA-mediated decomposition in THF, high concentrations of NaDA in THF should on a percentage basis decompose marginally more slowly.
(15) Kofron, W. G.; Baclawski, L. M. A Convenient Method for Estimation of Alkyllithium Concentrations. *J. Org. Chem.* **1976**, *41*, 1879.
(16) We cannot rule out the possibility that the C- and O-alkylation products from $BrCH_2COO$-*t*-Bu stem from enolization and attack on a transiently formed carbene. In fact, sequential addition of $BrCH_2COO$-*t*-Bu followed by pseudoephedrine amide **1** to excess NaDA afforded a seemingly similar product distribution.
(17) Langer, P.; Freiberg, W. Cyclization Reactions of Dianions in Organic Synthesis. *Chem. Rev.* **2004**, *104*, 4125.
(18) (a) Renny, J. S.; Tomasevich, L. L.; Tallmadge, E. H.; Collum, D. B. Method of Continuous Variations: Applications of Job Plots to the Study of Molecular Associations in Organometallic Chemistry. *Angew. Chem., Int. Ed.* **2013**, *52*, 11998. (b) Liou, L. R.; McNeil, A. J.; Ramírez, A.; Toombes, G. E. S.; Gruver, J. M.; Collum, D. B. Lithium Enolates of Simple Ketones: Structure Determination Using the Method of Continuous Variation. *J. Am. Chem. Soc.* **2008**, *130*, 4859.
(19) (a) Friebolin, H. *Basic One- and Two-Dimensional NMR Spectroscopy*; Wiley VCH: Weinheim, 2010. (b) Claridge, T. D. W. *High-Resolution NMR Techniques in Organic Chemistry*, 2nd ed.; Elsevier: Amsterdam, 2009.
(20) Frisch, M. J.; Trucks, G. W.; Schlegel, H. B.; Scuseria, G. E.; Robb, M. A.; Cheeseman, J. R.; Zakrzewski, V. G.; Montgomery, J. A., Jr.; Stratmann, R. E.; Burant, J. C.; Dapprich, S.; Millam, J. M.; Daniels, A. D.; Kudin, K. N.; Strain, M. C.; Farkas, O.; Tomasi, J.; Barone, V.; Cossi, M.; Cammi, R.; Mennucci, B.; Pomelli, C.; Adamo, C.; Clifford, S.; Ochterski, J.; Petersson, G. A.; Ayala, P. Y.; Cui, Q.; Morokuma, K.; Malick, D. K.; Rabuck, A. D.; Raghavachari, K.; Foresman, J. B.; Cioslowski, J.; Ortiz, J. V.; Baboul, A. G.; Stefanov, B. B.; Liu, G.; Liashenko, A.; Piskorz, P.; Komaromi, I.; Gomperts, R.; Martin, R. L.; Fox, D. J.; Keith, T.; Al-Laham, M. A.; Peng, C. Y.; Gill, A.; Nanayakkara, C.; Gonzalez, M.; Challacombe, P. M. W.; Johnson, B.; Chen, W.; Wong, M. W.; Andres, J. L.; Gonzalez, C.; Head-Gordon, M.; Replogle, E. S.; Pople, J. A. *Gaussian 09*, revision A.02; Gaussian, Inc.: Wallingford, CT, 2009.
(21) Zhao, Y.; Truhlar, D. G. The M06 Suite of Density Functionals for Main Group Thermochemistry, Thermochemical Kinetics, Noncovalent Interactions, Excited States, and Transition Elements: Two New Functionals and Systematic Testing of Four M06-Class Functionals and 12 Other Functionals. *Theor. Chem. Acc.* **2008**, *120*, 215.
(22) For leading references to marked enolate aging effects, see ref 5.
(23) The intended mole fraction refers to the mole fraction based on what was added to the samples. The measured mole fraction, the mole fraction within only the ensemble of interest, eliminates the distorting effects of impurities.
(24) For representative examples of crystallographically characterized stacked cubes of sodium salts, see: (a) Balloch, L.; Drummond, A. M.; García-Álvarez, P.; Graham, D. V.; Kennedy, A. R.; Klett, J.; Mulvey, R. E.; O'Hara, C. T.; Rodger, P. J.; Rushworth, I. D. Structural Variations Within Group 1 (Li- Cs)$^+$(2, 2, 6, 6-Tetramethyl-1-piperidinyloxy)$^-$ Complexes Made via Metallic Reduction of the Nitroxyl Radical. *Inorg. Chem.* **2009**, *48*, 6934. (b) Boyle, T. J.; Velazquez, A. T.; Yonemoto, D. T.; Alam, T. M.; Moore, C.; Rheingold, A. L. Synthesis and Characterization of a Family of Solvated Sodium Aryloxide Compounds. *Inorg. Chim. Acta* **2013**, *405*, 374. (c) Scherpf, T.; Wirth, R.; Molitor, S.; Feichtner, K. S.; Gessner, V. H. Bridging the Gap Between Bisylides and Methandiides: Isolation, Reactivity, and Electronic Structure of an Yldiide. *Angew. Chem., Int. Ed.* **2015**, *54*, 8542.
(25) Laube, T.; Dunitz, J. D.; Seebach, D. On the Interaction between Lithium Enolates and Secondary Amines in Solution and in the Crystal. *Helv. Chim. Acta* **1985**, *68*, 1373.
(26) Casado, J.; Lopez-Quintela, M. A.; Lorenzo-Barral, F. M. The Initial Rate Method in Chemical Kinetics: Evaluation and Experimental Illustration. *J. Chem. Educ.* **1986**, *63*, 450.
(27) The rate law provides the stoichiometry of the transition structure relative to that of the reactants: The rate law provides the stoichiometry of the transition structure relative to that of the reactants: Edwards, J. O.; Greene, E. F.; Ross, J. From Stoichiometry and Rate Law to Mechanism. *J. Chem. Educ.* **1968**, *45*, 381.
(28) Semilog plots, although often visually retrievable, can hide subtleties such as nonzero intercepts and impose inadvertent nonlinear weighting of the data.
(29) We define the idealized rate law as that obtained by rounding the observed reaction orders to the nearest rational order.
(30) A number of general-purpose reviews on determining reaction mechanism: (a) Meek, S. J.; Pitman, C. L.; Miller, A. J. M. Deducing Reaction Mechanism: A Guide for Students, Researchers, and Instructors. *J. Chem. Educ.* **2016**, *93*, 275. (b) Simmons, E. M.; Hartwig, J. F. On the Interpretation of Deuterium Kinetic Isotope Effects in C-H Bond Functionalizations by Transition Metal Complexes. *Angew. Chem., Int. Ed.* **2012**, *51*, 3066. (c) Collum, D. B.; McNeil, A. J.; Ramírez, A. Lithium Diisopropylamide: Solution Kinetics and Implications for Organic Synthesis. *Angew. Chem., Int. Ed.* **2007**, *46*, 3002. (d) Algera, R. F.; Gupta, L.; Hoepker, A. C.; Liang, J.; Ma, Y.; Singh, K. J.; Collum, D. B. Lithium Diisopropylamide: Non-Equilibrium Kinetics and Lessons Learned about Rate Limitation. *J. Org. Chem.* **2017**, *82*, 4513.
(31) Williard, P. G. unpublished.
(32) (a) Rong, Y.; Palmer, J. H.; Parkin, G. Benzannulated tris(2-Mercapto-1-imidazolyl)-hydroborato Ligands: Tetradentate κ4-S3H Binding and Access to Monomeric Monovalent Thallium in an [S3] Coordination Environment. *Dalton Trans* **2014**, *43*, 1397. (b) Peng, H.; Zhang, Z.; Qi, R.; Yao, Y.; Zhang, Y.; Shen, Q.; Cheng, Y. Synthesis, Reactivity, and Characterization of Sodium and Rare-Earth Metal Complexes Bearing a Dianionic N-Aryloxo-Functionalized r-Ketoiminate Ligand. *Inorg. Chem.* **2008**, *47*, 9828. (c) Bachmann, J.; Hodgkiss, J. M.; Young, E. R.; Nocera, D. G. Ground- and Excited-State Reactivity of Iron Porphyrinogens. *Inorg. Chem.* **2007**, *46*, 607.
(33) Representative examples of structurally characterized bridging THF ligands: (a) Chivers, T.; Fedorchuk, C.; Parvez, M. Synthetic and Structural Investigations of Monomeric Dilithium Boraamidinates and Bidentate NBNCN Ligands with Bulky N-Bonded Groups. *Inorg. Chem.* **2004**, *43*, 2643. (b) Briand, G. G.; Chivers, T.; Parvez, M. A Novel Route to Chalcogenides of Heavy Pnicogens: Synthesis and X-ray Structure of $\{(THF)_3Li_2[PhAs(Se)(NBu^t)_2]\}$. *J. Chem. Soc., Dalton Trans.* **2002**, 3785.
(34) Hoepker, A. C.; Collum, D. B. Computational Studies of Lithium Diisopropylamide Deaggregation. *J. Org. Chem.* **2011**, *76*, 7985.
(35) Chakrabarti, P.; Dunitz, J. D. Directional Preferences of Ether O-Atoms Towards Alkali and Alkaline Earth Cations. *Helv. Chim. Acta* **1982**, *65*, 1482.
(36) Intrinsic reaction coordinate (IRC) calculations are defined as "the minimum energy reaction pathway (MERP) in mass-weighted cartesian coordinates between the transition state of a reaction and its reactants and products." They show the minima preceding and following transition state.
(37) Grabowski, E. J. J. Reflections on Process Research—The Art of Practical Organic Synthesis. In *ACS Symposium Series, 870*; Abdel-Magid, A. F., Ragan, J. A., Eds.; American Chemical Society: Washington, DC, 2004; Chapter 1, pp 1–21.
(38) For leading references to structural studies of dianions, see ref 5.

DOI: 10.1021/jacs.9b08176
J. Am. Chem. Soc. XXXX, XXX, XXX−XXX